Front. Chem. Sci. Eng. 2019, 13(4): 672–683
https://doi.org/10.1007/s11705-019-1856-6

RESEARCH ARTICLE

Encapsulation of 2-amino-2-methyl-1-propanol with tetraethyl orthosilicate for CO_2 capture

Sidra Rama[1], Yan Zhang[1], Fideline Tchuenbou-Magaia[2], Yulong Ding[1], Yongliang Li (✉)[1]

1 School of Chemical Engineering, University of Birmingham, Edgbaston, Birmingham B12 2TT, UK
2 School of Engineering, University of Wolverhampton, Wolverhampton WV1 1LY, UK

Abstract Carbon capture is widely recognised as an essential strategy to meet global goals for climate protection. Although various CO_2 capture technologies including absorption, adsorption and membrane exist, they are not yet mature for post-combustion power plants mainly due to high energy penalty. Hence researchers are concentrating on developing non-aqueous solvents like ionic liquids, CO_2-binding organic liquids, nanoparticle hybrid materials and microencapsulated sorbents to minimize the energy consumption for carbon capture. This research aims to develop a novel and efficient approach by encapsulating sorbents to capture CO_2 in a cold environment. The conventional emulsion technique was selected for the microcapsule formulation by using 2-amino-2-methyl-1-propanol (AMP) as the core sorbent and silicon dioxide as the shell. This paper reports the findings on the formulated microcapsules including key formulation parameters, microstructure, size distribution and thermal cycling stability. Furthermore, the effects of microcapsule quality and absorption temperature on the CO_2 loading capacity of the microcapsules were investigated using a self-developed pressure decay method. The preliminary results have shown that the AMP microcapsules are promising to replace conventional sorbents.

Keywords carbon capture, microencapsulated sorbents, emulsion technique, low temperature adsorption and absorption

1 Introduction

The global industrialization and growing population have brought a yearly increase in energy consumption. The estimated global energy-related emission increase is predicted to be 3.7 Gt of CO_2 by 2030 [1]. The increase of CO_2 emission into the environment has contributed to global warming as well as climate change which is a primary concern today. In the foreseeable future, fossil fuels will still be used for most of electrical power generation and industrial manufacturing in many countries [2]. Scientists speculate that at least 69% of CO_2 emission and 60% of greenhouse gases are produced through energy generation, whereas 80% of the world energy is derived from fossil fuel. The International Agency has reported a 6% increase in CO_2 emission every two years due to the dependency of the world economy on fossil fuels for an energy source. Even the Nobel Prize-winning Intergovernmental Panel have concerns and advise that a cut of 50%–80% is required by 2050 to avoid the most harmful effects of climate change [3]. Furthermore, industries such as refinery plants, ammonia synthesis plants and hydrogen manufacturers also require the removal of CO_2 to prevent the corrosion of pipeline, catalyst poisoning and clogging due to dry ice formation. One of the most promising approaches to tackle the high emission rate of CO_2 is the use of carbon capture and storage technology, which aims at capturing CO_2 from power stations and other industrial facilities, compressing, and then transporting it to underground storage locations.

Although various CO_2 capture technologies exist (Fig. 1), post-combustion CO_2 capture is the most mature technique including absorption, adsorption and membrane [4–8]. However, these technologies are not mature enough to be used in power plants due to mass transfer limitation in the sorption processes that occur with high flue gas quantity as well as high energy demand during the regeneration process. Hence researchers are concentrating on developing non-aqueous solvents like ionic liquids, CO_2-binding organic liquids, nanoparticle hybrid materials and microencapsulated sorbents due to their potential of being more energy saving and environmentally friendly [9].

The most established CO_2 absorption technique during post-combustion is the contact of an aqueous amine with

Received October 3, 2018; accepted March 2, 2019

E-mail: y.li.1@bham.ac.uk

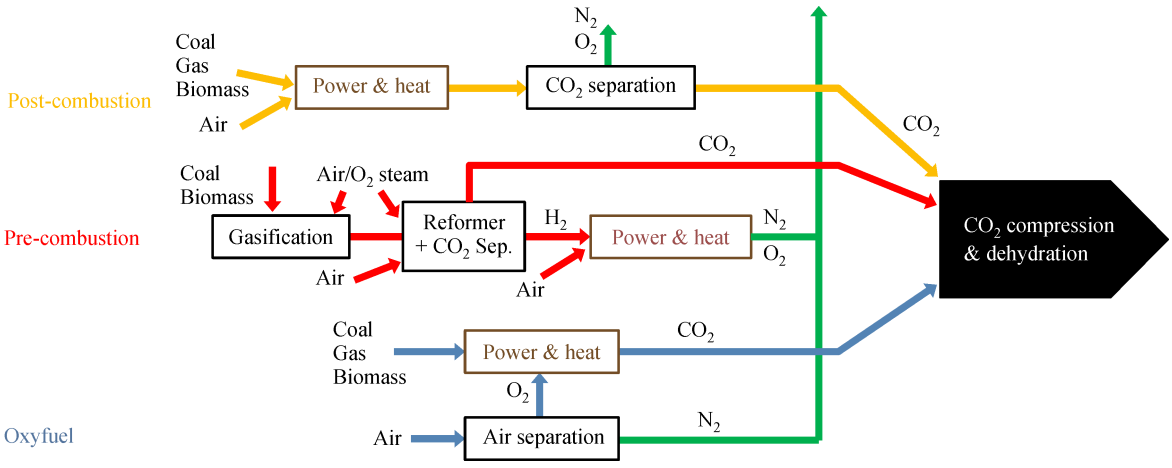

Fig. 1 Illustration of the different pathways for CO_2, N_2 and O_2 separation [10].

flue gas to form carbamates as the amine reacts with CO_2. The commonly used amine is monoethanolamine (MEA) which has a high absorption rate and loading capacity. However, drawbacks such as high corrosivity, toxic degrading side-products and high amount of energy required for CO_2 removal during the sorbent regeneration prevent its widespread use. Thus, new sorbents are proposed to overcome these limitations by combining the liquid sorbents (core) with solid ones (shell) thereby forming microcapsules. The liquid solvent would provide high capacity, selectivity as well as water tolerance, whereas the solid sorbents would provide a high surface and in turn higher absorption capacity as well as low volatility [11]. Moreover, microencapsulation can also lower the cost of CO_2 capture by containing precipitates, and isolate the solvent from reactor equipment [12].

Microencapsulation is defined by either enveloping or surrounding one substance within a different substance at a small scale to yield micro-sized capsules. The micro-encapsulated material has limitless applications such as pharmaceuticals, cosmetics, textiles, agriculture, foods, paints, coatings and fragrances [13]. The microcapsule can vary in shape from spheres with a core surrounded by a continuous wall to asymmetrical with various shapes containing embedded droplets of core material throughout the capsules. Hence, it can provide more comfortable handling of liquid and gas material as solids, while allowing a measure of protection against hazardous material handling. In the case of carbon capture, the microcapsules can offer the potential of combining chemical absorption of CO_2 with physical adsorption. Chemical absorption creates chemical bonding between the chemical solvent and the captured CO_2, whereas the physical adsorption allows gas permeation or desorption into solid/ liquid under specific conditions. Temperature and pressure control the rate of desorption or absorption and therefore, eliminate the need for the production of hazardous products.

In recent years, microcapsules composed of liquid carbonate cores and silicone shells have been produced using a microfluidic device. The idea was to link the liquid sorbents selectivity and capacity with the high surface area of the capsules for fast and controlled CO_2 absorption and desorption over multiple cycles. Their study reported a lower mass transport across the capsule shell compared to conventional liquid sorbents. However, the enhanced surface area gained through encapsulation delivered an increase in CO_2 absorption rate for the given sorbent mass [11]. Another study by the same research group demonstrated an increased rate of CO_2 absorption by a factor of 3.5 with encapsulated ionic liquids in a silicon shell, when compared to a liquid film. However, these solvents are highly viscous or change phases, posing challenges for conventional process equipment [14].

In the present study 2-amino-2-methyl-1-propanol (AMP) is used instead as the core sorbent as it is of low viscosity, easy to process and has high CO_2 sorption capacity. Our research aims to produce porous micro-capsules with highly permeable shells and high sorption capacity core for efficient CO_2 capture using conventional formulation technology. As a widely known method for microencapsulation, the emulsion technique was chosen for the encapsulation process due to the potential of encapsulating hydrophobic and hydrophilic substances [15,16]. The effect of stirring speed during formulation, thermal properties, the payload of the formulated micro-capsules, as well as sorption capacity of the produced microcapsules, were investigated as well for its potential industrial applications. The results are expected to provide an alternative CO_2 absorption technique to the current CO_2 capture technologies.

2 Materials and methods

2.1 Chemicals

AMP (> 98%) is chosen as the core materials; Tetraethyl

orthosilicate (TEOS, > 99%) is chosen as the shell material due to its high permeability to gases, compatibility with the core as well as immiscibility with the formulation oil. Other chemicals used in the formulation process include thymol blue, polyglycerol polyricinoleate (PGPR, > 99%) and mineral oil (> 99%) (Table 1). All these chemicals were purchased from Sigma Aldrich, UK.

Table 1 Important features of the materials used for microencapsulation

Function	Material	Features
Core	AMP	Highest CO_2 loading capacity, low regeneration temp
Shell	TEOS	Permeability to gas
Immiscible phase	Mineral oil	Immiscibility with core

2.2 Formulation of microcapsules

The microencapsulation process includes the emulsion of AMP into a mineral oil followed by the polymerization of the silica precursors to form the shell as shown in Fig. 2. During core preparation, 15 g of the colorless, liquid AMP is mixed with 1 g of Thymol blue, a pH indicator, to give a blue colored AMP solution. The purpose of the dye is to enable qualitative analysis of CO_2 capture into the encapsulated AMP. Meanwhile, 10 g TEOS is mixed with 2 g of 0.5% sodium hydroxide (NaOH) to start the alkaline polymerization of the silica. In the formulation process, 70 g of mineral oil with 0.35% PGPR, a surfactant, is added to a jacketed beaker connected to a water bath. The temperature of the water bath is kept constant at 20°C throughout the whole encapsulation process. The oil is mechanically stirred (IKA). The AMP solution with the pH indicator is added to the oil phase by slow pipetting. Due to the immiscibility of the oil and core, small core droplets are formed, providing an interface for the TEOS particles in a later stage. Afterwards, activated TEOS is slowly pipetted into the oil phase. During the encapsulation, three different stirring speeds were used: (1) 100 r/min; (2) 400 r/min; and (3) 600 r/min, to formulate three samples (Sample 1, 2 and 3 respectively). During the formulation process, the whole system is covered up to prevent solvent evaporation. Furthermore, the whole process takes place under constant temperature and mechanical stirring for at least ⩾12 h. Afterwards, the sample is centrifuged and repeatedly washed with hexane (⩾99%) to remove excess oil, unencapsulated AMP, oligomers of TEOS particles and then vacuum dried. Once the microcapsules are successfully formulated, the sample is characterized and tested for CO_2 absorption.

2.3 Microcapsules characterization

The internal structure, morphology, size uniformity and aggregation of the formulated microcapsules were examined using scanning electron microscopy (Hitachi Tabletop TM3030 SEM) with backscattered electrons at 15 kV. The samples were coated with 3 nm gold (gold spluttering machine) before each test. The size distribution of the microcapsule was determined by utilising a Malvern MasterSizer 2000 that uses the static light scattering and

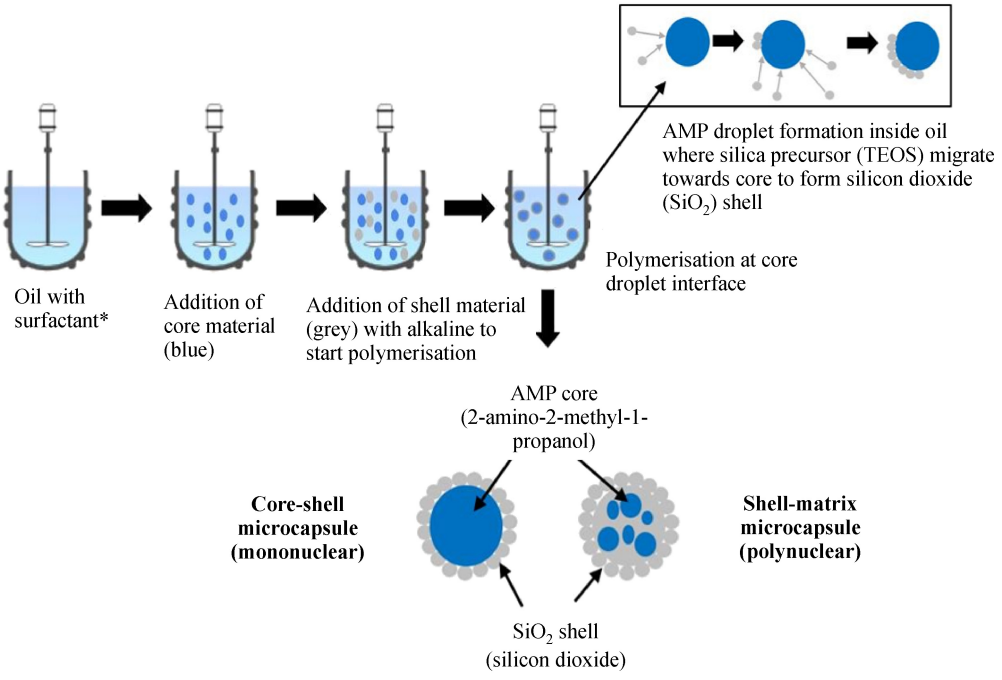

Fig. 2 Schematic diagram of the microencapsulation of AMP with TEOS (*varying stirring speeds used).

the Mie scattering theory. These theories assume that all particles are spherical with larger particles scatter light at a smaller angle than smaller ones. This MasterSizer used works in the size range of 0.02 to 2000 μm. To identify the microcapsule size, the refractive index of the shell and the solvent liquid needs to be known. The refractive index for both silicon dioxide and ethanol were taken from the literature and are 1.45 and 1.36, respectively. The results are shown as the average values of 3 data sets. The specific surface area (m^2/g), average pore volume (cm^3/g) and pore size (Å) of the formulated microcapsules were measured and calculated using a Bruner-Emmett-Teller (BET) instrument (Micrometrics TriStar II Plus). The sample was inserted into the instrument after a pretreatment under vacuum at room temperature to ensure that the sample is completely dried. The standard measurement points used were P/P_0 of 0.1, 0.2 and 0.3. The absorbed gas volume on particle surface was measured at the boiling point of nitrogen (–196°C). The amount of adsorbed and desorbed gas was then correlated to the total surface area including the pore volume and size at the surface. The calculated values are based on the BET theory. Gas adsorption also enables the determination of size and volume distribution of pores.

Thermal stability of the formulated microcapsules was investigated using differential scanning calorimetry (DSC2, STAR^e System; Mettler Toledo) and dilatometer. In DSC measurement the test temperature range was 25°C to −60°C. In dilatometer measurement 10 continuous thermal cycling between 25°C and −100°C were carried out and samples were then observed for any changes in physical properties such as shape and size. The chemical composition and stability of the formulated microcapsules were measured using Fourier transform infrared spectroscopy (FTIR) which can identify bonds present inside the samples [17]. For comparison purpose, the encapsulated sample was run against pure core material.

The payload (amount of AMP content inside the sample) of the formulated microcapsules was identified using a thermogravimetric analysis (Mettler Toledo). To this end, 10–20 mg of sample was heated above the boiling temperature of the core material (250°C for AMP), and the temperature is kept constant at that temperature for 2 h to evaporate all the core material. The payload is then calculated as follows:

$$\phi = \frac{m_I - m_S}{m_I} \times 100\%, \quad (1)$$

where ϕ is payload (wt-%); m_I is the initial weight of sample; m_S is the weight of shell after the core evaporation process.

2.4 CO_2 sorption process

A pressure rig was set up to test the CO_2 absorption loading capacity and kinetics of the microcapsules with the piping and instrumentation diagram (PID) is shown in the schematic diagram in Fig. 3. The sample holder in the pressure rig is a glass crucible to allow observation of the sample (quantitative analysis) from any perspective. Before exposing the sample to CO_2, the pressure rig chamber is vacuumed to ensure CO_2 sorption occurs when pressure is introduced. A circulating water bath connected to the pressure rig was used to ensure constant temperature

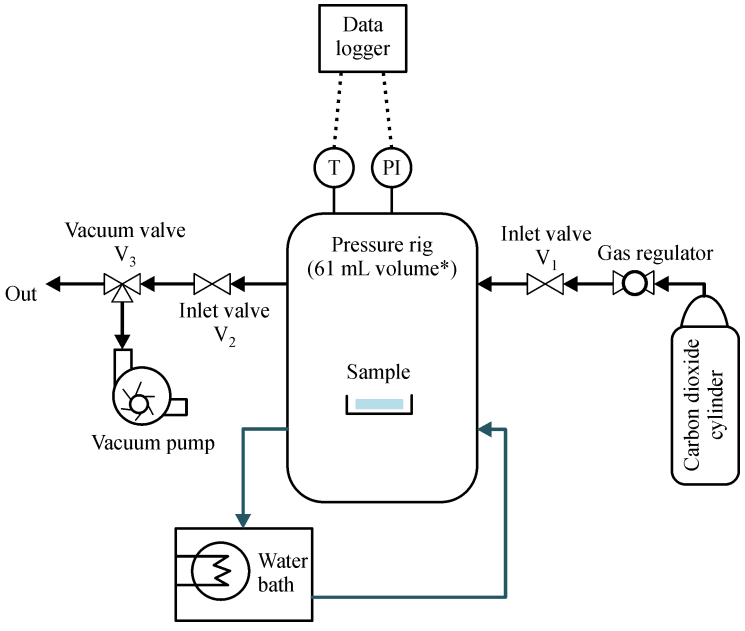

Fig. 3 Schematic diagram of pressure rig set-up for CO_2 absorption testing (* Effective volume of pressure rig = 61 mL, including pressure cell, connections, valves and tubings).

during the testing. A data logger records the pressure and temperature during the experiments. Pressure is measured by a transducer (Omega, model no: PX309-300AI) in volts with the Data Logger which is converted to Bara for CO_2 absorption calculations. At the end of the experiment, the sample was removed from the rig after depressurizing the vessel, and the sample is weighed for comparison of weight change.

For all CO_2 sorption experiments with the pressure rig, 0.5±0.01 g of the sample was used. The experiments were performed at 10 barA initial pressure and temperatures were maintained ranging from −40°C to 20°C (±0.1°C). Amount of CO_2 absorbed by the sample is calculated by the pressure drop over time using Peng Robinson equation of state. To validate the data, CO_2 sorption tests for each sample were repeated at least three times. Furthermore, the calculated values and the measured physical weight changes between before and after CO_2 exposure were compared. The CO_2 absorption system and sample loading capacity were considered valid only when the calculated values agreed with the physically measured values within a 5% error. For comparison purposes, images of the samples were also taken both before and after sorption.

3 Results and discussion

3.1 Formulation process and microcapsule quality

The most common precursors used for making silicon dioxide are silicon alkoxides which are characterized by the strong covalent Si–O bonding. These bonds are hydrophobic and thus immiscible with water. TEOS is such a silica precursor. The advantage of using TEOS as a precursor is its polymerization ability in alkaline, acidic and neutral conditions to form silicon dioxide. During formulation alkaline conditions were chosen due to the high alkalinity of the core material [18]. In this case the polymerization of TEOS would occur through alkaline catalyzed hydrolysis and condensation which are caused by the hydroxyl ions (OH^-) of the sodium hydroxide. These OH^- ions have a strong nucleophilicity and thus can attack the silicon atom. The alkoxide silicon atoms carry the highest positive charge and are therefore the target of the nucleophilic attack from the deprotonated hydroxyl ions (OH^-). This mechanism leads to the formation of a penta-coordinate intermediate [19]. The alkaline polycondensation of TEOS was initiated with sodium hydroxide first to form oligomers and then the silica particles to form the capsule shell (Fig. 4). The hydroxyl ions have a strong nucleophilicity to attack the silicon atom of TEOS as it carries the highest positive charge and therefore becomes the target [20]. Typically condensation nucleation occurs under mild to extreme alkaline conditions [21,22].

This *in-situ* polymerization is a two-step process as it involves the preparation of the pre-condensate by adding sodium hydroxide to TEOS. This is then followed by the encapsulation of the core material under alkaline environment. This two-step process is necessary for the shell formation and cannot be achieved with a one-step *in-situ* polymerization [23]. The *in-situ* polymerization produces porous, spherical shaped microcapsules with a matrix internal structure rather than a core-shell type matrix as can be seen in Fig. 5 and Fig. 6, called monolithic (matrix) microcapsules due to the migration of the activated TEOS towards the AMP interface inside the oil. However, due to the force created by the mechanical stirrer the shell particles come into contact to form a stable polymeric system, leading to a more or less uniform core material distribution across the polymer matrix. Another possible reason could be the reactivity of the hydroxyl (–OH) group of AMP with the activated TEOS forming bonds which leads to the core material distribution inside the polymer matrix. This core distribution may be in micronised particle form or particles with a substantial fraction of the microcapsule itself [24]. From the view of applications, the advantage of these matrix microcapsules is the ruggedness where the dissolution properties are less likely to be either affected or altered by the abrasion or pressure [25], whereas the core-shell capsule would suggest a higher CO_2 loading capacity on the other hand [20,21].

It can be seen from Fig. 6 that the morphology of the microcapsules does not vary much from each other with the various stirring speeds used. The samples only differ in the amount of agglomeration present inside each sample. Sample 1 produced with the lowest stirring speed shows the highest particle attachement on capsule surface compared to the other 2 samples. The main disadvantage of the *in-situ* polymersiation is that it takes place inside an emulsion where the polymerisation can only be controlled to a small degree. This leads to traces of monomers and oligomers of TEOS to be found with the final product

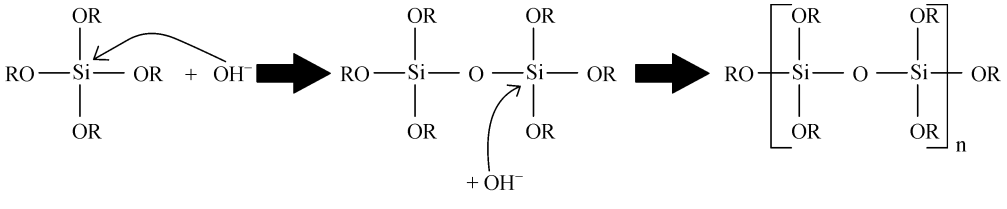

Fig. 4 Polycondensation of TEOS with hydroxyl ions [21], where R represents the alkyl group, C_2H_5.

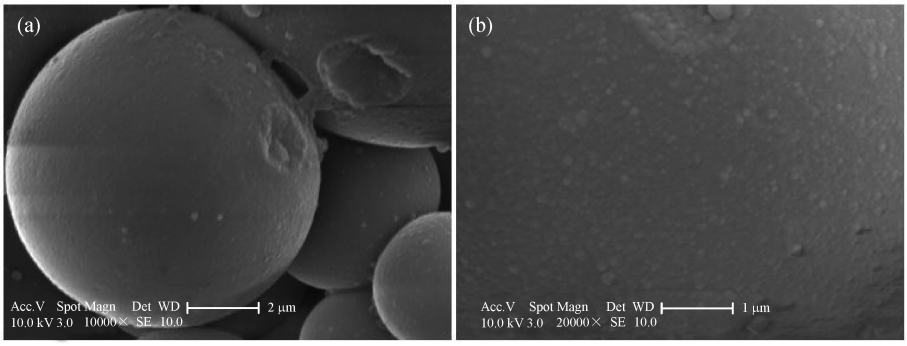

Fig. 5 Surface structure of microcapsules (TM3030). (a) Surface Structure of microcapsules; (b) high magnification of microcapsule surface.

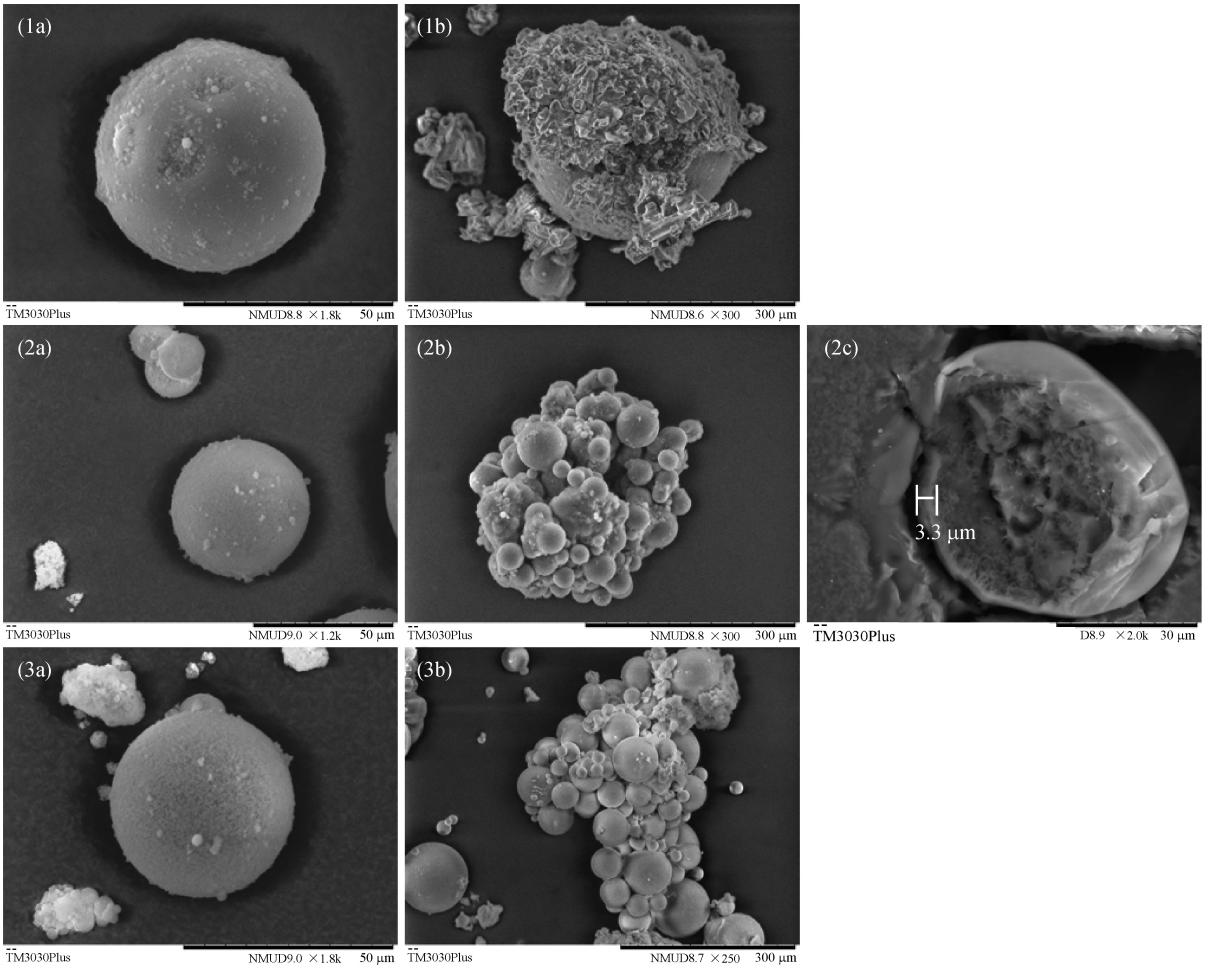

Fig. 6 Morphology of microcapsules with AMP as core and silica as a shell. (1a) Sample 1: single microcapsule; (1b) Sample 1: single microcapsule with agglomeration; (2a) Sample 2: single microcapsule; (2b) Sample 2: Microcapsule with agglomeration, (2c) Sample 2: broken microcapsule for shell thickness example; (3a) Sample 3: single microcapsules; (3b) Sample 3: microcapsule with agglomeration.

which are very hard to remove from the sample. This is one of the causes that leads to sample agglomeration [25] which is seen in the SEM images (Fig. 6). Furthermore, this method leads to a thin microcapsule shell formation (3.3 μm as shown in Fig. 6 (2c)) with high permeability which works well during the experimental CO_2 sorption tests. Theoretically, a thinner shell might be preferrable due to the faster CO_2 kinetics it could provide. However, the

CO_2 absorption results presented in the present work demonstrate a right balance between sorption kinetics and shell thickness as would be discussed in the following.

Surface area (SA) and pore size are both important physical properties that impact the absorption capacity of the microcapsules. The difference in the porosity and SA of particles with otherwise same physical dimension greatly influences the sample characteristics. During the formulation different stirring speeds were used to produce microcapsules, where each speed produces different sized particle and hence gives each sample a different surface erea, as shown in Table 2. Comparing the pore size of all the samples, they can be classified as mesoporous in size (20–500 Å) [26]. However, the samples differ in their specific SA, where sample 2 has much higher SA with 92 m^2/g than the other two samples partially due to its highest pore volume (0.09792 cm^3/g) and lowest average pore size (43 Å). It has to be kept in mind that during the BET adsorption the material surface is assumed to be homogeneous whilst the adsorption is equal across the entire surface. However, the samples formulated contain agglomeration and particle attachment which can be seen in the SEM images (Fig. 6), suggesting that both inter and intra pore volume cannot be differentiated from each other. In this case the agglomeration and particle attachment seem to decrease the surface area of a sample due to particles most likely covering the pores on the capsule surface [26].

The SA differences also agree with the particle size distribution of the individual samples as represented by Fig. 7. It can be seen that sample 3 has the smallest overall capsule size with the narrowest size distrbution (5–40 μm) out of all the three samples. In comparison, sample 1 yielded the largest capsules with the broadest size distribution among all the samples. The mean particle size for the various samples were 140, 105 and 20 μm for sample 1, 2 and 3, respectivley. These differences in the size distribution inside the samples occur due to the force created by the mechanical stirrer that involves core drop breakup by generated shear stresses. These stresses are not uniform across the system, hence the highly polydispersed samples. As the stirring speed is increased from 100 to 600 r/min, smaller microcapsules with smaller size distribution but high agglomeration are produced (sample 3), as higher stirring speed causes the internal phase into smaller droplets, thus, decreasing the mean diameter of the formed microcapsules [27,28]. On the other hand, at lower stirring speed the broader size distribution causes more particle attachment as can be observed in sample 1. This indicates that an optimal stirring speed is an important factor to improve the microcapsule quality in the formulation process.

3.2 Thermal properties and chemical composition

The thermal properties of the formulated microcapsules were compared against the pure core material to observe the effect of encapsulation on the core material, specifically microcapsule thermal stability at low temperature. It can be seen from Fig. 8 that pure, liquid AMP shows a freezing point at −22°C, whereas the second peak at −16°C and

Table 2 Specific surface area, pore volume and average pore size of sample 1, 2 and 3

Sample	BET surface area /($m^2 \cdot g^{-1}$)	Pore volume /($m^2 \cdot g^{-1}$)	Average pore size /Å
1	29	0.051	71
2	92	0.097	43
3	34	0.061	72

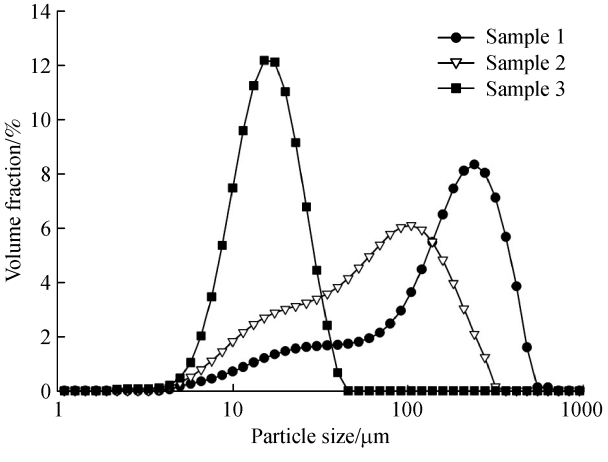

Fig. 7 Comparison of stirring speed effect on particle size distribution.

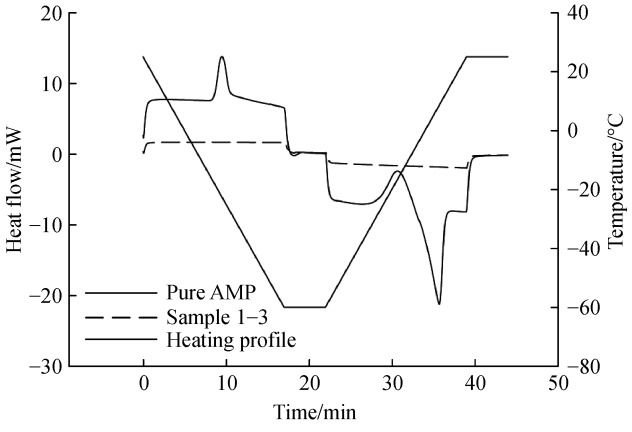

Fig. 8 Thermal property comparison of pure AMP (liquid) against the encapsulated sample 1, 2 and 3.

the third one at 8°C representing the recrystallisation and melting respectively. It is worth mentioning that no freezing point has been stated in literature to the best of our knowledge for AMP; only a melting temperature of 30°C–31°C [29]. However, according to the DSC result (Fig. 8) for pure, liquid AMP the freezing point seems to be around −22°C, suggesting the material undergoes crystallization at this point. The endothermic peak (melting of material) around 8°C is also not found in literature which is explained by the re-melting of the AMP from the crystalline state that shifts the melting point of the material to a lower temperature. These results suggest possible changes in material properties compared to pure, liquid core.

In comparison, no melting or freezing is observed with encapsulated samples irrespective of their stirring speed, indicating good thermal stability over the range of 25°C to −60°C which is supported by the findings of the SEM images (Fig. 9). The thermal cycling of all three samples show no change in morphology after ten continuous cycling of 20°C to −100°C which was carried out with a dilatometer. These results indicate that all produced microcapsules irrespective of their stirring speed can withstand very low temperature whilst still being able to retain their shape after intensive, low temperature exposure, though some microcapsules occasionally do show cracks and dents.

The chemical composition analysis of the formulated microcapsules was carried out using FTIR, indicating possible amine reacting during polymerization and as a result the creation of new bonds as well as the decrease of core concentration. It can be seen from Fig. 10 that the pure, liquid core material (AMP) has an overall higher IR transmittance compared to the encapsulated sample, this is especially the case for 3000–3500 cm^{-1} IR spectra range. The primary interest in the FTIR spectra is the N–H bonds from the amine groups and the O–H bonds from the propanol groups. Both the N–H bonds and the O–H bond are present in the FTIR spectra (Fig. 10) in the range of 3500–3200 cm^{-1}, making it harder to distinguish between the two bonds as they have overlapping infrared transmittance absorbance. However, the bimodal nature of the first two peaks, suggests the presence of primary amines whereas the third peak suggests the hydroxyl group [30]. The N–H bond stretch transmittance in the range of 3250 to 3650 cm^{-1} decreases after encapsulation, which is suggesting a reduction in the free AMP due to polymerisation reaction between the amine and shell material [30]. This reduction in AMP is not favorable because it would affect the CO_2 absorption as less AMP is available to react with CO_2 to form carbamate ions. However, the most likely reason for the reduced peaks compared to the pure liquid AMP is due to a lower amount of the encapsulated solvent. Though there is the possibility of *in-situ* polymerisation of the amine group from AMP [31], amine and the hydroxyl group (–OH) both have the same probability of providing the required hydrogen for the formation of the shell material.

3.3 CO_2 Absorption

Samples exposed to CO_2 undergo a color change from blue to yellow which is shown in Fig. 11 suggests carbamate formation [32,33] and provides evidence of successful CO_2 absorption by the samples. The change in color occurs due to the presence of Thymol Blue inside the microcapsules. This method of visual CO_2 absorption has also been used by Aines et al. [34] where sample color changed when up to ~90% of maximum carbon uptake reached. This visible color enables qualitative evaluation of the CO_2 absorption and desorption capacity of microcapsules. The pH of the sample before testing was > 10 due to high alkalinity of AMP but drops to < 6 after the absorption as carbamate ions are formed while hydrogen ions are released [32]. This chemical absorption process is a widely known method and is under consideration for an industrial scale CO_2 capture system [35].

Moreover, this carbamate reaction is reversible as shown in Fig. 12. The thermal regeneration heat requirement is dependent on the energy required to break the bonds that were created during the CO_2 absorption. The lower the required energy, the lower the energy-intensive CO_2 release process [35,36]. In our case when the microcapsules are heated up to 40°C slightly higher than the

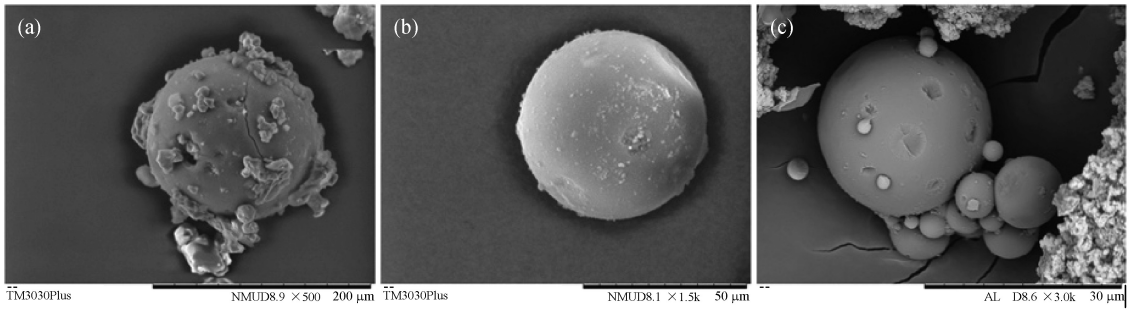

Fig. 9 Microcapsule morphology after ten continuous cycling. (a) Sample 1: microcapsule with crack and dents; (b) Sample 2: microcapsules with dents; (c) Sample 3: microcapsule with dents.

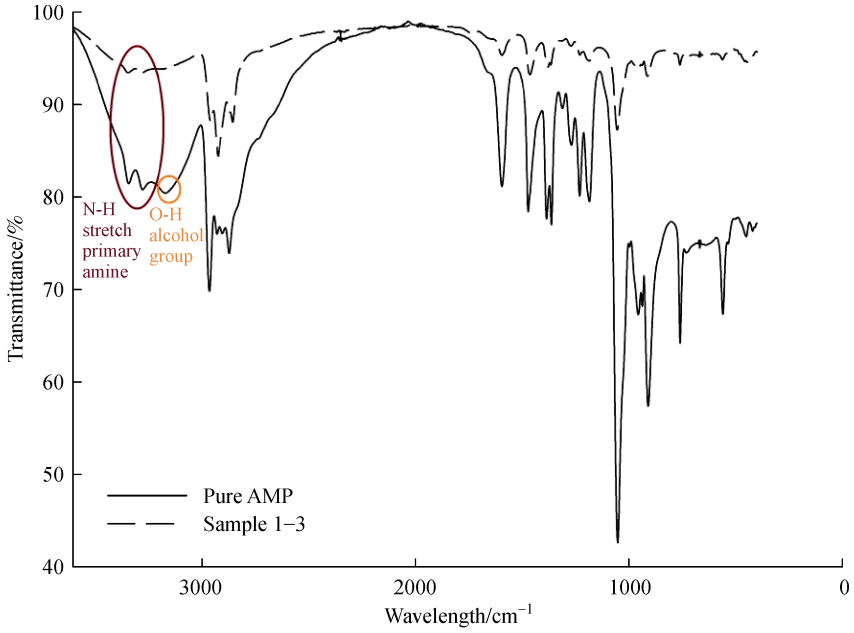

Fig. 10 FTIR spectra of pure, liquid AMP and encapsulated AMP. Samples 1–3 represented as on graph due to same transmittance. The area of interest is indicate.

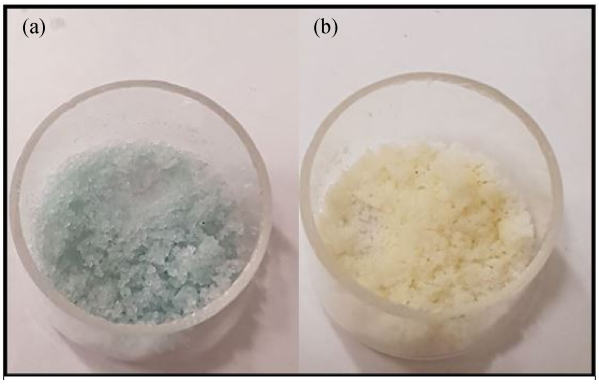

Fig. 11 Color change of sample from (a) blue to (b) yellow after CO_2 exposure.

melting point, the color changes back to light blue, suggesting the release of CO_2. In comparison with an aqueous amine scrubbing, a mature CO_2 absorption process, the presented approach is by far less energy intensive in regeneration which can take up ⩾80% of the energy cost saving [34].

To analyse the type of reaction happening during CO_2 absorption, the temperature curve of both sample and control was recorded while the rig is initially pressurised with 10 barA. In Fig. 13 an increase in temperature is observed for both sample and control during the absorption tests after pressure is introduced inside the rig chamber. A second smaller temperature increase of 0.5°C is observed only with the sample after the initial drop. The temperature and pressure stabilise over time for both samples. This result indicates that the CO_2 absorption and thus the carbamate formation is of exothermic nature.

As soon the pressure is introduced into the chamber the sample starts to absorb the CO_2. This fact, however, is negligible for the pressure to CO_2 absorption conversion as it only takes 1–2 min for the pressure to stabilize. Furthermore, this method relies on the pressure stabilization after initial pressure introduction into the chamber for the absorption conversion which is related to the temperature. Temperature increases as a consequence of pressurizing the vessel as both influence each other. A temperature increase can lead to an increase in pressure and vice versa. Therefore, it was necessary to record absorption data only after temperature stabilization.

As the system is completely sealed off and no leakage is occurring, the sample absorbs CO_2 and hence leads to a drop in pressure. Therefore, the absorbed CO_2 by the sample was calculated by converting the pressure drop into mass gained by the sample with the help of the Peng Robinson Equation of State. To validate the calculated CO_2 absorption capacity of the samples at the end of an experiment, each sample was weighed before and after CO_2 absorption and the two values were compared. The results were considered only when the calculated values were within 5% error margin of the physical weight.

All three samples showed similar sorption behavior with an initial rapid sample weight increase which is then followed by a continuous, slow CO_2 uptake. However, comparing the three samples regarding CO_2 absorption at room temperature, sample 2 shows the highest CO_2 loading capacity of 0.19 g/g sample, followed by

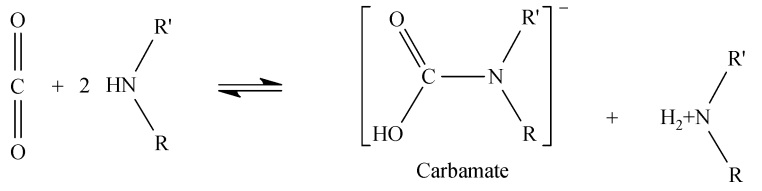

Fig. 12 Reversible carbamate reaction.

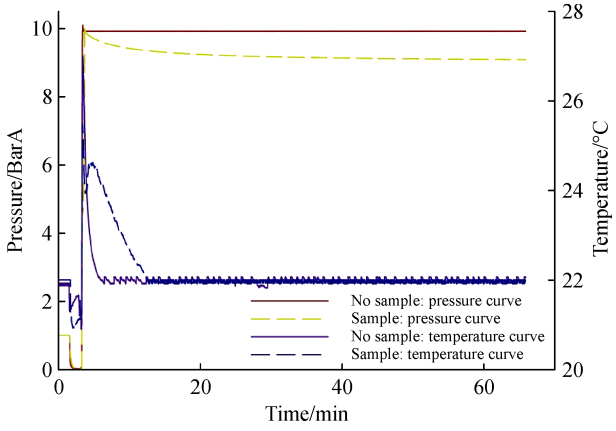

Fig. 13 Pressure behaviour comparison of control and sample 2.

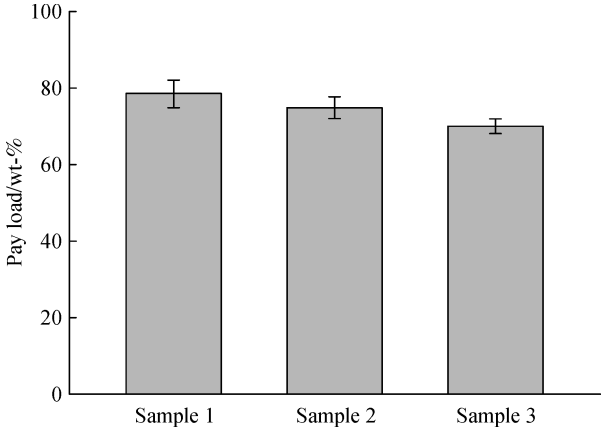

Fig. 15 Pay load of encapsulated sample in wt-%.

0.18 g/g of sample 1 and 0.16 g/g of sample 3, as shown in Fig. 14, while the absorption capacity of pure AMP is 0.29 g/g. It indicates that both particle size distribution as well as surface area play important roles in the absorption capacity.

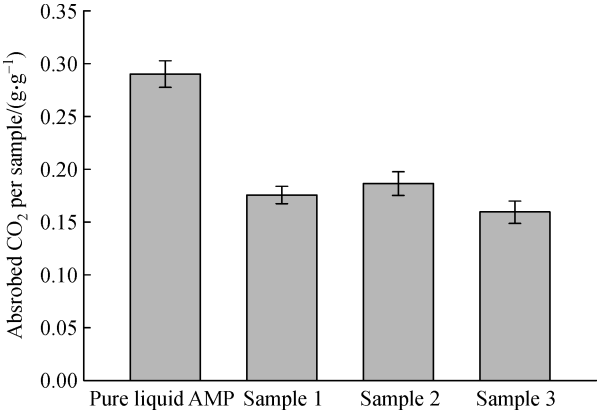

Fig. 14 Carbon dioxide absorption comparison of encapsulated sample against pure core material.

Figure 15 shows the pay load of the individual samples. As expected sample 1 has the highest pay load of about 78% due to the largest particle size of 140 μm, while sample 3 has the lowest pay load of about 70% on average. This, however, is not reflected in the absorption graph shown in Fig. 14. Linking the SA to the absorption capacity, it can be concluded that even if the pay loads are similar, capsules with higher surface area are more intimate in contact with the gas and thus increase the absorption capacity which is the case for sample 2. On the other hand, if similar surface areas are similar (samples 1 and 3 as indicated in Table 2), capsules with higher pay load affirmatively have higher absorption. The experimental results confirm that sample 2 displays the best balance between its surface properties and pay load resulting the highest absorption capacity.

The effect of temperature on CO_2 absorption capacity was also observed for the three samples. It can be seen from Fig. 16 that the absorption capacity for pure core material (AMP) decreases from 0.31 to 0.28 g/g sample

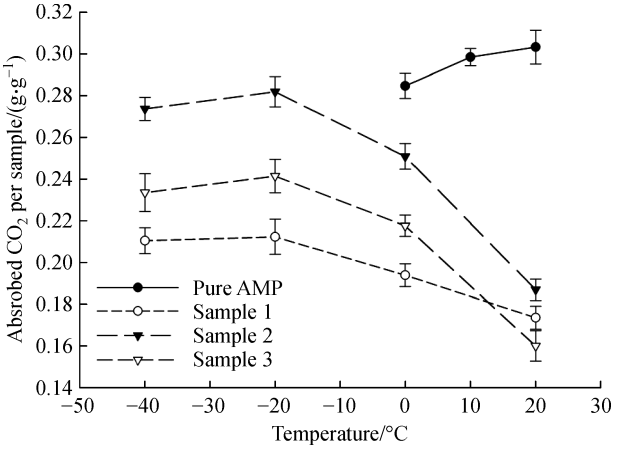

Fig. 16 Effect of temperature on absorption capacity.

corresponding to the temperature drop from 20°C to 0°C. In contrast, the encapsulated sample shows an increase in absorption capacity as temperature decreases, e.g., absorption capacity of sample 2 increases from 0.19 g/g sample at 20°C to 0.28 g/g sample at −40°C. It indicates that physical absorption seems take over the chemical absorption at lower temperature while chemical absorption slows down due to a decrease in kinetic energy and as a result of slower diffusion (which is the case with the pure core material). However, for physical adsorption, the surface area is of more importance and hence why a higher absorption was seen at a lower temperature. The absorption capacity only increases up to −20°C, suggesting the maximum absorption capacity is reached for all samples. Comparing the absorption capacity of sample 1 and 3 with each other, sample 3 initially has the lowest capacity at room temperature with 0.16 g/g sample but steadily increases to 0.23 g/g sample as the temperature decreases due to the higher surface area to volume ratio and higher pore volume, giving the sample higher physical adsorption on the surface. In contrast sample 2 shows the highest CO_2 absorption capacity, suggesting the best balance between the core material and surface area to volume ratio. This result proves that lowering the temperature has a positive effect on the absorption capacity of the microencapsulated AMP [37,38].

Overall, the experimental CO_2 capacity of the microcapsules with AMP core shows a lower absorption capacity compared to the literature value. However, the CO_2 absorption capacity of the AMP microcapsules is equivalent to the pure MEA solvents, showing a promising future for the AMP microcapsules [39].

4 Conclusions

Microcapsules formulated with AMP as the core sorbent and silicon dioxide as the shell were successfully produced using conventional emulsion method and in situ polymerization. The produced microcapsules were uniformly shaped, with a smooth, porous surface and shown good thermal and cycling stability atributed to the matrix like-structure which is less sensitive to stresses compared to core shell structures. It is found that the stirring speed is a key formulation factor to balance the surface properties and payload of the formulated AMP microcapsules, which are of importance for the CO_2 absorption capacity. Specifically, in the present case a stirring speed of 400 r/min gives formulated microcapsules the largest surface area of 92 m^2/g with highest pore volume of 0.097 cm^2/g and the lowest average pore size of 43 Å. Although the pay load of this sample is slightly lower than that of sample obtained from a lower stirring speed (100 r/min, 78%), the CO_2 absorption capacity is the highest of the three samples with 0.19 g of CO_2 absorbed per 1 g of sample. Moreover, it is also demonstrated that lower temperature increases the absorption capacity of all the AMP microcapsules samples significantly due to better physical adsorption instead of chemical absorption. Again, it turns out the surface properties of microcapsules play a more important role in the improvement at lower temperatures.

Acknowledgements The authors gratefully acknowledge the financial support of the Engineering and Physical Science Research Council (EPSRS) of the United Kingdom under the grants EP/N000714/1 and EP/N021142. We would also like to thank our colleagues at the Birmingham Centre for Energy Storage (BCES) for their expertise and insight that assisted the research.

References

1. Florin N, Fennell P. Carbon capture technology: Future fossil fuel use and mitigating climate change. Grantham Institute Climate Change Brief Paper, 2010, 3(3): 20
2. Anderegg W R L, Prall J W, Harold J, Schneider S H. Expert credibility in climate change. Environmental Sciences, 2010, 107(27): 12107–12109
3. Plasynski S I, Chen Z Y. Review of CO_2 capture technologies and some improvement opportunities. ACS Division of Fuel Chemistry. Preprints, 2000, 45: 644–649
4. Zou J, Ho W S W. CO_2-selective polymeric membranes containing amines in crosslinked poly(vinyl alcohol). Journal of Membrane Science, 2006, 286(1-2): 310–321
5. Tuinier M J, Hamers H P, Van Sint Annaland M. Techno-economic evaluation of cryogenic CO_2 capture: A comparison with absorption and membrane technology. International Journal of Greenhouse Gas Control, 2011, 5(6): 1559–1565
6. Li P, Tezel F H. Equilibrium and kinetic analysis of CO_2-N_2 adsorption separation by concentration pulse chromatography. Journal of Colloid and Interface Science, 2007, 313(1): 12–27
7. Li M, Jiang X, He G. Application of membrane separation technology in postcombustion carbon dioxide capture process. Frontiers of Chemical Science and Engineering, 2014, 8(2): 233–239
8. Desideri U. Advanced absorption processes and technology for carbon dioxide (CO_2) capture in power plants. In: Developments and Innovation in Carbon Dioxide (CO_2) Capture and Storage Technology. Woodhead Publishing Limited, 2010, 155–182
9. Dai Z, Noble R D, Gin D L, Zhang X, Deng L. Combination of ionic liquids with membrane technology: A new approach for CO_2 separation. Journal of Membrane Science, 2016, 497: 1–20
10. Liu G X. Greenhouse gases—capturing, utilization and reduction.

InTechOpen, 2012: 1–24.
11. Vericella J J, Baker S E, Stolaroff J K, Duoss E B, Hardin J O, Lewicki J, Glogowski E, Floyd W C, Valdez C A, Smith W L, Satcher J H, Bourcier W L, Spadaccini C M, Lewis J A, Aines R D. Encapsulated liquid sorbents for carbon dioxide capture. Nature Communications, 2015, 6(1): 6124
12. Davidson R M. Post-combustion carbon capture—solid sorbents and membranes. Energy Procedia, 2013, 37: 134–141
13. Peanparkdee M, Iwamoto S, Yamauchi R. Microencapsulation: A review of applications in the food and pharmaceutical industries. Reviews in Agricultural Science, 2016, 4(0): 56–65
14. Stolaroff J K, Ye C, Oakdale J S, Baker S E, Smith W L, Nguyen D T, Spadaccini C M, Aines R D. Microencapsulation of advanced solvents for carbon capture. Faraday Discussions, 2016, 192(0): 271–281
15. Jyothi Sri S, Seethadevi A, Suria Prabha K, Muthuprasanna P, Pavitra P. Microencapsulation: A review. International Journal of Pharma and Bio Sciences, 2012, 3(1): 509–531
16. Shah R K, Shum H C, Rowat A C, Lee D, Agresti J J, Utada A S, Chu L Y, Kim J W, Fernandez-Nieves A, Martinez C J, Weitz D A. Designer emulsions using microfluidics. Materials Today, 2008, 11(4): 18–27
17. Nielsen C J, Herrmann H, Weller C. Atmospheric chemistry and environmental impact of the use of amines in carbon capture and storage (CCS). Chemical Society Reviews, 2012, 41(19): 66–84
18. Shimekit B, Mukhtar H. Natural gas purification technologies—major advances for CO_2 separation and future firections. In: Advances in Natural Gas Technology. InTechOpen, 2012, 235–270
19. Harrod J F, Laine R M. Applications of organomettallic chemistry in the preparation and processing of advanced materials. Kluwer Academic Publishers, 1995, 3–25
20. Innocenzi P. The Sol to Gel Transition. Berlin: Springer, 2016, 7–25
21. Bhakta S, Dixit C K, Bist I, Jalil K A, Suib S L, Rusling J F. Sodium hydroxide catalyzed monodispersed high surface area silica nanoparticles. Materials Research Express, 2016, 3(7): 1–14
22. Brinker C J. Hydrolysis and condensation of silicates: Effects on structure. Journal of Non-Crystalline Solids, 1988, 100(1-3): 31–50
23. Wang R, Li H, Liu W, He X. Surface modification of poly(urea-formaldehyde) microcapsules and the effect on the epoxy composites performance. Pure and Applied Chemistry, 2010, 47(10): 991–995
24. Kuriokase A B, Padma S, Padma Priya S. A Review on microcapsules. Global Journal of Pharmacology, 2015, 9(1): 28–39
25. Tarcha P J. Polymers for Controlled Drug Delivery. Florida: CRC Press, 1991: 286
26. Lowell S, Shields J E, Thomas M A, Thommes M. Characterisation of Porous Solids and Powders: Surface Area, Pore Size and Density. Berlin: Springer, 2004, 58–81
27. Vysloužil J, Doležel P, Kejdušová M, Mašková E, Mašek J, Lukáč R, Košťál V, Vetchý D, Dvořáčková K. Influence of different formulations and process parameters during the preparation of drug-loaded PLGA microspheres evaluated by multivariate data analysis. Acta Pharmaceutica (Zagreb, Croatia), 2014, 64(4): 403–417
28. Tamilvanan S, Sa B. Effect of production variables on the physical characteristics of ibuprofen-loaded polystyrene microparticles. Journal of Microencapsulation, 1999, 16(4): 411–418
29. Chan C, Maham Y, Mather A E, Mathonat C. Densities and volumetric properties of the aqueous solutions of 2-amino-2-methyl-1-propanol, *n*-butyldiethanolamine and *n*-propylethanolamine at temperature from 298.15 to 353.15 K. Fluid Phase Equilibria, 2002, 198(2): 239–250
30. Majury T G. Amines and carboxylic acids as initiators of polymerization in caprolactam. Journal of Polymer Science. Polymer Physics Edition, 1958, 31(123): 383–397
31. Wan Isahak W N R, Che Ramli Z A, Mohamed Hisham M W, Yarmo M A. The formation of a series of carbonates from carbon dioxide: Capturing and utilisation. Renewable & Sustainable Energy Reviews, 2015, 47: 93–106
32. Nair P S, Selvi P P. Absorption of carbon dioxide in packed column. International Journal of Science Research Publication, 2014, 4(1): 2250–3153
33. Vericella J J, Baker S E, Stolaroff J K, Duoss E B, Hardin J O, Lewicki J, Glogowski E, Floyd W C, Valdez C A, Smith W L, et al. Encapsulated liquid sorbents for carbon dioxide capture. Nature Communications, 2015, 6(1): 6124
34. Aines R D, Spaddaccini C M, Duoss E B, Stolaroff J K, Vericella J, Lewis J A, Farthing G. Encapsulated solvents for carbon dioxide capture. Energy Procedia, 2013, 37: 219–224
35. Stephens J C, Van Der Zwaan B, Kennedy J F. CO_2 capture and storage (CCS): Exploring the research, development, demonstration, and deployment continuum. Energy Technology Innovation Project. Harvard University, 2005, 3–20
36. Fredriksen S B, Jens K J. Oxidative degradation of aqueous amine solutions of MEA, AMP, MDEA, Pz: A review. Energy Procedia, 2013, 37: 1770–1777
37. Nicholas B P, Lu Y. CO_2 absorption into concentraed carbonate solutions with promoters at elevated temperatures. Dissertation for the Master's Degree. Illinois: University of Illinois, 2014: 3–10
38. Haslam T B R, Hershey R L, Keen R H. Industrial and engineering chemistry. Effect of gas velocity and temperature on rate of absorption. UTC, 2018, 18: 41
39. Wang T, Jens K J. Oxidative degradation of AMP/MEA blends for post-combustion CO_2 capture. Energy Procedia, 2013, 37: 306–313